Asian Journal of Chemistry; Vol. 33, No. 4 (2021), 712-726

ASIAN JOURNAL OF CHEMISTRY

https://doi.org/10.14233/ajchem.2021.23027

Coral Limestone Modified by Magnetite and Maghemite Nanocomposites for Sequestration of Lead(II) and Chromium(VI) Ions from Aqueous Solution

C.S. NKUTHA*, N.D. SHOOTO and E.B. NAIDOO

Applied Chemistry and Nano Science Laboratory, Department of Chemistry, Vaal University of Technology, P.O. Box X021, Vanderbijlpark, 1900, South Africa

*Corresponding author: E-mail: cynthiankutha61@gmail.com

Received: 14 October 2020; *Accepted*: 5 January 2021; *Published online*: 20 March 2021; AJC-20272

In present work, a one pot synthesis of magnetic nanocomposites was synthesized by using co-precipitation method in air atmosphere. The synthesis of magnetite and maghemite supported on biogenic coral limestone was done by varying the ratio of Fe(II)/Fe(III) in solution to obtain the two phases of iron oxide and capping with sucrose in air atmosphere. The nanocomposites were characterized by FTIR, where the results showed a distinct peak for Fe-O, while UV/vis showed an absorption in the visible region which is typical of iron oxide. Photoluminescence results showed that the nanocomposites were both red shifted for magnetite-PCLS (PCLS = pristine coral limestone) and magnetite-CCLS (CCLS = calcined coral limestone); while a blue shift and red shift was observed for the maghemite-PCLS and maghemite-CCLS. From the SEM a deviation of sphericity of the nanocomposites, with maghemite having an uneven distribution was observed. Equilibrium was reached within 60 min, of which maghemite showed higher metal uptake. The kinetic data fit PSOM better as compared to PFOM, this means that adsorption was due to the charge density on the surface of the nanocomposites. The good fit for intraparticle diffusion (IPD) also suggested that adsorption was also observed due to mass transfer, it was observed that the rate limiting step was due to surface adsorption. This was in good correlation with the better fit of PSOM. The mechanism of adsorption was found to be better explained by physisorption and the surface was heterogeneous whereby multilayer adsorption was possible. The data was also subjected to Dubinin-Radushkevich isotherm, which suggests that the uptake of the pollutants was due to physisorption. The adsorption process was spontaneous and favourable which is supported by the negative values of Gibb's free energy for the system.

Keywords: Magnetite, Maghemite, Nanocomposite, Pristine coral limestone, Calcined coral limestone, Adsorption.

INTRODUCTION

The contamination of water has been a growing concern for millennia and surface water is threatened by the rise in water pollution throughout the world [1,2]. Toxic pollutants are poisonous and pose a health risk to whatever they come into contact [3]. The growth of industrial activities since the first industrial revolution, has spiked an increase in manufacturing which has led to anthropogenic water pollution. This has been due to the unlawful discharge of untreated water from industry into surface water [4]. This activity has led to a number of ecosystems left in distraught, with communities battling with the ramifications of such activities [5].

Toxic pollutants such as heavy metal ions have detrimental effects even at low concentrations, this is due to their ability to accumulate in living organisms [6]. Lead(II) is a non-essential metal and toxic. Exposure to lead(II) has been associated with physiological problems such as hypertension, anaemia, nephropathy, decreased growth, hearing loss, effects on the reproduction and development [7-10]. It is used in industries such as ceramics, pigments and paint, casting metals and battery manufacturing [11]. Chromium exists as two main dominant oxidation states Cr(III) and Cr(VI) [12,13], with a high solubility and mobility of Cr(VI), which can easily pass through cell membranes hence it has been labelled as a carcinogen and teratogen [14]. Chromium is used in many applications in industries such as electroplating, development of pigments, leather processing, stainless steel and non-iron alloys [15].

The remediation of contaminated water is of importance, especially in light of pandemics such as the novel Covid-19 whereby the importance of washing hands with clean water has been highlighted. Over the years the treatment of contami-

nated water has been done using a variety of methods such as adsorption [7], chemical precipitation [16], solvent extraction [17] and ion exchange [18]. In comparison to these methods adsorption has been widely studied globally due to its advantageous characteristics, which include lower cost from the process and maintenance, efficiency, removal of toxic pollutants even at low concentrations without production of secondary pollutants and the ability to regenerate the adsorbent and recover the adsorbate [19].

Adsorption requires an adsorbent that has a high surface area which will be able to immobilize the toxic pollutants by various mechanisms [20]. Many commercially available adsorbents are unviable due the high cost they introduce into the process and large consumption of energy. Activated carbon is an example of such adsorbents, which requires energy consuming processes such as pyrolysis which contribute to the large carbon footprint, while some naturally occurring adsorbents degrade over time [21]. Today, much research has been conducted whereby biomass from a wide range of sectors has been explored for the development of adsorbents [22,23].

The development of adsorbents from biomass has been studied for their potential use in toxic metal remediation. The successful development and applications of nano magnetic materials has created interest in the revival of biomass as potential adsorbents [24-27]. This has been due to the need for finding low cost materials that meet environmental remediation needs, with regard to removal that is efficient and not selective [7]. Synthetic magnetite has been widely studied due to its natural counterpart that is naturally occurring and one of the most abundant material on earth. To maintain the use of low cost in adsorbent development whilst increasing the adsorptive capacity, incorporation of biomass with magnetite has been studied.

Magnetite can be synthesized using various ways such as sol-gel method [28], co-precipitation [29], ball milling [30] and ultrasound methods [31]. Among these methods, co-precipitation is widely used due to the simplicity of the method, energy efficient, ability to control the variables easily such pH which affects the size and distribution of the formed nanocomposites and ability to use low temperature [32]. The as-synthesized nanocomposites must have a high surface area, zero coercity so they can be superparamagnetic and must be monodispersed; although polydispersed nanocomposites have also been found to be effective [33,34]. Superparamagnetic magnetite and maghemite have been widely used in different field depending on their characteristics. In environmental research more specifically in water treatment, surface area and recovery of the adsorbent has been the driving force for use of superparamagnetic nanocomposites [35].

One of the main issues which are associated with magnetic nanocomposites are aggregation due to dipole-dipole attraction which leads to colloidal growth by reducing surface area and increasing the particle size [36,37]. An increase in size would diminish the magnetic characteristics of the nanocomposites [38], therefore making them unfavourable for many applications. This has led to surface supported synthesis of magnetic nanocomposites by utilizing different surfactants with capping properties [39]. The surfactant must be able to reduce the metal ions into atoms and provide steric hindrance so as to avoid attraction from the particles on the surface of the nanocomposites [37,40].

Different biopolymers have been used during synthesis of magnetic nanocomposites to offer support. Biopolymers are important because they produce nanocomposites that are biocompatible, superparamagnetic and stable in both air and water [39,41]. Aghazadeh *et al.* [42] successfully synthesized stable superparamagnetic magnetite due to surface coated from vitamin C and sucrose. The synthesized nanocomposites were found to meet the criteria for biomedical applications. Hoang *et al.* [43] impregnated snail shell with Fe_3O_4 at different ratios, for the removal of Cr(VI). Panneerselvan *et al.* [24] impregnated tea wastes with Fe_3O_4 for the removal of Ni(II), their results showed that an increase in concentration of Ni(II) from 50 ppm to 100 ppm decrease the uptake of the magnetized tea wastes from 96 to 87%, the equilibrium was reached with 120 min.

Coral limestone have shown unprecedented capabilities as an adsorbent, this has been shown in earlier works by Samadi *et al.* [44] who removed As(V) by using pristine and treated coral limestone. The experimental procedure showed removal capacity of 99.2 and 91.2%, respectively. Shokohi *et al.* [45] studied the removal of Pb(II) and Cd(II) of which they observed 8.14 and 5 mg/g pollutant removal, respectively. Malakootian *et al.* [46] removed reactive red 198 dye by using coral limestone and they obtained a removal capacity of 19.83 mg/g. Nkutha *et al.* [47,48] removed Pb(II), Cr(VI) and methylene blue dye using pristine coral limestone with metal uptake capacities of 39.26, 69.42 and 37.24 mg/g, respectively.

Furthermore, a modification of the coral limestone with an acid and base resulted in uptake capacities of 74.11, 65.04 and 46.28 mg/g for Pb(II), Cr(VI) and methylene blue dye onto the acid modified coral limestone and 78.34, 64.88 and 46.39 mg/g for Pb(II), Cr(VI) and methylene blue dye onto the base modified coral limestone. The above literature therefore suggests that the coral limestone can be used as adsorbents in water and wastewater treatment plants for heavy metal removal. However, the scope of research is too limited thus further development and knowledge is required. Therefore, this study introduces the adsorption of Pb(II) and Cr(VI) using modified coral limestones by a one pot synthesis of magnetite and maghemite. To the best of our knowledge, no study has reported on the synthesis of magnetic coral limestone and its application for the removal of Cr(VI) and Pb(II) from aqueous solution.

Coral limestone is made up of biogenic $CaCO_3$ in the aragonite polymorph [49], the combination of $CaCO_3$ and calcined $CaCO_3$ for the synthesis of magnetite and maghemite is to provide strength, support, durability and stability to the magnetic nanocomposites [50]. For a greener method, this one pot synthesis will be supported by sucrose a non-reducing sugar, which acts as a support and a capping agent for the nanocomposites and solubilizer for $CaCO_3$ and calcined $CaCO_3$ [51]. In alkaline conditions sucrose hydrolyses leading to the release of the reducing sugars glucose and fructose, aiding in a decreased particle growth by preventing aggregation in the nanocomposites [52,53].

EXPERIMENTAL

Preparation of adsorbents

Preparation of pristine coral limestone biomass (PCLS): Coral limestone were washed several times with deionized water to remove sand and excess salt. They were then dried in an oven at 40 ºC for 12 h and ground by a blender with steel blades. The ground material was sieved on 60/200 mesh to obtain approximate particle sizes between 0.8 and 1 mm. The sieved material was stirred in distilled water then dried at 40 ºC overnight. Thereafter, the dried material was labelled (PCLS).

Synthesis of magnetite-PCLS: PCLS was mixed with 100 mL of 1 mol L^{-1} sucrose in a beaker under stirring for 0.5 h. The Fe(II) and Fe(III) in a ratio of 3:1 were added to the PCLS sucrate mixture. Then 25 mL of 25% NH_4OH was introduced dropwise followed by the immediate formation of a black slurry. The pH of the mixture was adjusted to pH = 14 by addition of 0.1 NaOH. The reaction was allowed to mix for 6 h under air atmosphere. The final black slurry was maintained at pH =14, then washed once with distilled water and three times with absolute ethanol to remove any unreacted substances on the surface of the nanocomposites and dried at 75 ºC for 120 h. The obtained material was designated as magnetite-PCLS.

Synthesis of maghemite-PCLS: PCLS was mixed with 100 mL of 1 mol L^{-1} sucrose in a beaker under stirring for 0.5 h. The Fe(II) and Fe(III) in a ratio of 2:1 were added to the calcium sucrate mixture and 25 mL of 25% NH_4OH was introduced dropwise followed by the immediate formation of a black slurry. The pH of the mixture was adjusted to pH = 14 by addition of 0.1 NaOH. The reaction was allowed to mix for 72 h under air atmosphere. The final slurry was maintained at pH 14 and washed once with distilled water, three times with absolute ethanol and dried at 75 ºC for 24 h resulting in curry coloured solid. The obtained material was designated as maghemite-PCLS.

Preparation of calcined coral limestone (CCLS): PCLS was calcined in a furnace at 900 ºC for 1 h, this was allowed to return to room temperature over a period of 24 h. The calcined sample was then further dried at 50 ºC for 2 h. The obtained material was designated as CCLS900.

Synthesis of magnetite-CCLS: CCLS900 was mixed with 100 mL of 1 mol L^{-1} sucrose in a beaker under stirring for 30 min at room temperature. The Fe(II) and Fe(III) in a ratio of 3:1 were added to the CCLS900 sucrate mixture. A 25 mL of 25% NH_4OH was introduced dropwise followed by the immediate formation of a black slurry which over time became a curry brown. The pH of the mixture was adjusted to pH = 14 by addition of 0.1 M NaOH. The reaction was allowed to mix for 6 h under air atmosphere. The final black slurry was maintained at pH =14, washed once with distilled water and three times with absolute ethanol then dried at 75 ºC for 120 h. The dried material was designated magnetite-CCLS.

Synthesis of maghemite-CCLS: CCLS900 was mixed with 100 mL of 1 mol L^{-1} sucrose in a beaker under stirring for 0.5 h at room temperature. The Fe(II) and Fe(III) in a ratio of 2:1 were added to the calcium sucrate mixture. A 25 mL of 25% NH_4OH was introduced dropwise followed by the immediate formation of a black slurry which over time became a curry brown. The pH of the mixture was adjusted to pH = 14 by addition of 0.1 M NaOH. The reaction was allowed to mix for 72 h under air atmosphere. The final slurry was maintained at pH = 14, washed once with distilled water and three times with absolute ethanol then dried at 75 ºC for 24 h resulting in a curry coloured solid. The obtained material was designated maghemite-CCLS.

Adsorption experiments: Adsorption studies were done in batch experiments by varying parameters such as agitation time (5-120 min), concentration (20-200 mg/L), pH (2, 4, 6, 8 and 10) and temperature (289, 299 and 309 K). The adsorbents mass was kept constant at 10 mg, stock solutions of 1000 mg/L were prepared, namely Pb(II) and Cr(VI) from the prepared stock solutions a working standard of 100 mg/L was prepared. Adsorption was carried out in a 50 mL centrifuge tube with 20 mL of solution added, under agitation at 200 rpm. After each experiment, the respective centrifuge bottles were removed and centrifuged for 5 min at 4000 rpm, the supernatants were analyzed using AAS.

Data analysis: The adsorption capacities (q_e) of adsorbents towards Pb(II) and Cr(VI) were evaluated by eqn. 1, where C_o and C_e are the initial and final concentrations of Pb(II) and Cr(VI) in the solution in (mg/L); V is the volume of the solution in (mL) and m is the mass of the adsorbents in (mg).

$$q_e = \frac{(C_o - C_e)V}{m} \quad (1)$$

Kinetics, pseudo-first order (PFO), pseudo-second order (PSO) and intraparticle diffusion (IPD) models were evaluated by eqns. 2-4, respectively. In PFO and PSO equations, (q_e) is the amount of total Pb(II) and Cr(VI) adsorbed in (mg/g) at time (t). PFOM rate constant (k_1) in (1/min) and PSOM rate constant (K_2) in (g/mg min). IPDM rate constant (k_i) in (g/g min); (C) is the amount of Pb(II) and Cr(VI) on the adsorbent surface. Kinetic models were evaluated by nonlinear equations introduced into KyPlot software.

$$q_e = q_t(1 - e^{-k_1 t}) \quad (2)$$

$$q_e = \frac{1 + k_2 q_e t}{k_2 q_e^2 t} \quad (3)$$

$$q_t = k_i(t^{1/2}) + C \quad (4)$$

Adsorption isotherms (Langmuir and Freundlich models) were evaluated by eqns. 5 and 6, respectively. Langmuir 2, parameter (q_m) is the maximum adsorption capacity of the adsorbent in (mg/g), (C_e) is the maximum adsorption capacity at time t in (mg/g), (K_L) is the solute surface interaction energy constant. Freundlich, (k_f) is the capacity factor constant and (1/n) is the isotherm linearity parameter constant.

$$\frac{1}{q_m} = \left(\frac{1}{K_L q_m}\right)\frac{1}{C_e} + \frac{1}{q_m} \quad (5)$$

$$q_e = k_f C_e^{1/n} \quad (6)$$

Enthalpy change (ΔH^o), entropy change (ΔS^o) and free energy change (ΔG^o) were evaluated by eqns. 7 and 8 at 289, 299 and 309 K:

$$\ln K_c = -\frac{\Delta H^\circ}{RT} - \frac{\Delta S^\circ}{R} \quad (7)$$

$$\Delta G^\circ = -RT \ln K_c \quad (8)$$

(K_c) is the equilibrium constant of thermodynamic function. (K_c) values were calculated by means of eqn. 9:

$$K_c = \frac{q_e}{C_e} \quad (9)$$

Characterization: Scanning electron microscopy (SEM) was used to study the surface morphology of the nanocomposites. Atomic absorption spectroscopy (Shimadzu AA-7000, Japan) equipped with a lamp of tungsten and deuterium were used to provide illumination, using flame atomic absorption spectrophotometer for metal detection. Optical studies of the nanocomposites were studied using a Thermo scientific Evolution UV visible spectrophotometer, collecting a spectre at λ = 1100-190 nm using a spectral bandwidth of 1 nm. Photolumiscent spectroscopy was used to analyze the electronic behaviour of the nanocomposites, using a Jasco Sprectro-Fluorimeter FP-8600 equipped with an XE lamp at 150 W and bandwidth of excitation at 5 nm with emission at 200-1010 nm. Perkin-Elmer Fourier transformed infrared spectroscopy FTIR/FTNIR spectrometer, spectrum 400 to 4000 nm was used. Point zero charge was done using an orbital shaker for 24 h, using the drift method and potassium nitrate salt.

RESULTS AND DISCUSSION

FTIR spectroscopy: Fig. 1 shows the FTIR spectra of the adsorbents, the formation of a calcium sucrose adduct through the hydroxyl bonding was confirmed by the presence of shifted peaks at wavenumber 1083 cm^{-1} for magnetite-PCLS, 1481 cm^{-1} for magnetite-CCLS, 1397 cm^{-1} for maghemite-PCLS and 1041 cm^{-1} for maghemite-CCLS which is assigned to C-O as observed by Tajmir-Riarhi [53]. The presence of the magnetic Fe-O nanoparticles at wavenumber 550 cm^{-1} was attributed to the symmetric stretching of Fe-O in that region [42,54]. The absence of the ring deformation of sucrose in the region 1100-500 cm^{-1} which was distinctive of vibrations by C-O-C, C-C-C and C-C-C-H confirms that the ring structure of sucrose was not deformed [52]. The absorption peak at 998 to 1393 cm^{-1} is attributed to the C-O and C-OH stretching, which were comparable to Sivakumar *et al.* [55] even though the peaks of maghemite-PCLS is shifted. The absorption peak at wavenumber 1888-1870 cm^{-1} was attributed to the carbonyl group C=O of either sucrose, glucose or fructose, which was also found by Agudelo *et al.* [56] when they used sucrose to obtain silver and gold nanoparticles. The corresponding peaks in 2084 and 2949 cm^{-1} are attributed to the variable and weak symmetric and asymmetric stretching of CH_2 and C-H which are distinctive to sucrose [53]. The peak at 2380 cm^{-1} is attributed to the combination of physically adsorbed and gaseous CO_2 [57], which could be due to the synthesis of the magnetic nanoparticles in air atmosphere. The absorption peak at 3610 cm^{-1} is due to the adsorbed water on the surface of the materials [52].

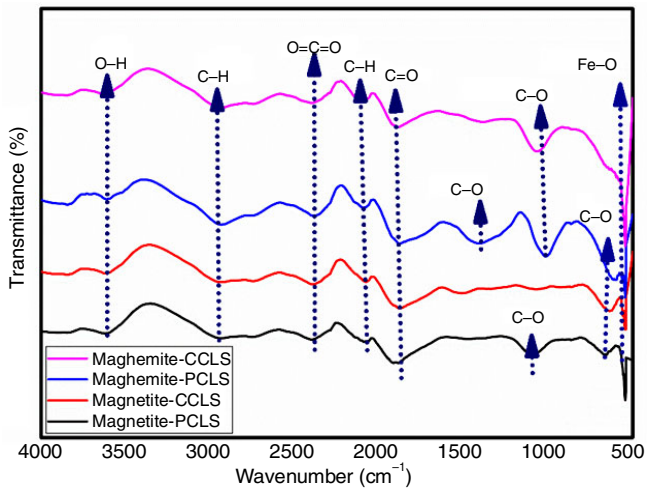

Fig. 1. FTIR spectroscopy of magnetite-PCLS, magnetite-CCLS, maghemite-PCLS and maghemite-CCLS

Scanning electron microscope: The SEM images of the synthesized magnetic nanocomposites was done to assess the surface of the materials. Fig. 2 depicts the SEM results, it was observed that the materials are not single crystals, this assumes that during their synthesis the nucleation process was random. Hence the formation of randomly orientated crystals exhibited a polycrystalline nature observed for all the materials. The magnetite-PCLS (Fig. 2a-b) show a much grainy surface structure which has a higher sphericity as compared to magnetite-CCLS. The surface image of the magnetite-PCLS is similar to that obtained by Doyle *et al.* [58], which confirmed a calcite phase based on the surface morphology. The particles are randomly organised with poor sorting in terms of size. Magnetite-PCLS (Fig. 2a-b) showed more consistency in terms of the structure of the grains in comparison with magnetite-CCLS (Fig. 2c-d). The structure of magnetite-CCLS lacked sphericity and a crystal shape, it has random shapes which are completely unsorted and appear to be fragmented which also indicated a polycry-stalline nature. However, the surface of magnetite samples (Fig. 2a-d) slightly differs from that of maghemite, in that the grains on maghemite (Fig. 2e-i) seem to have attached to them much smaller particles, but they still exhibit a polycrystalline nature. The maghemite-PCLS sample was observed to have sphericity which is between low and moderate, the randomly shaped nanocrystals were poorly sorted with the coarse grains domi-nating on the surface. However, it was observed that on top of the coarse grains, there were smaller grains which are visible on the materials surface. The distribution of the nanocrystals onto maghemite-CCLS was also randomly shaped with the more spherically related nanocrystal dominating. The sorting of the surface was also random, it was also observed that the smaller grains which are evenly distributed on the surface of the material are also dominating on top of the coarse grains.

UV/vis spectroscopy: Optical studies were evaluated using UV/Vis spectra (Figs. 3a-d) The presence of more surface plasmon resonance is indicative of an anisotropic material with decreased sphericity as found on the surface of the materials by SEM analysis. The magnetic nanocomposites absorption

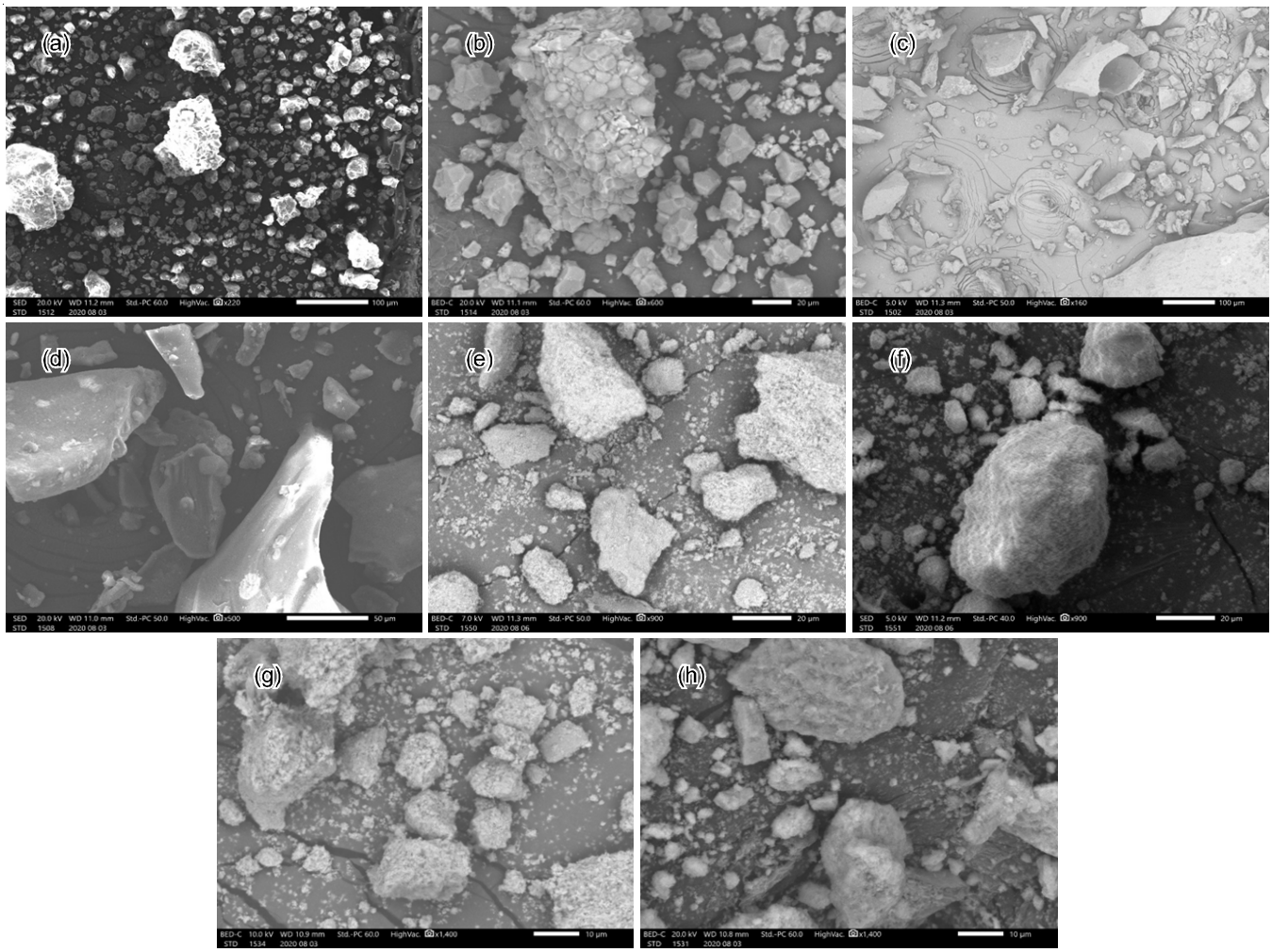

Fig. 2. SEM images of (a) magnetite-PCLS (b) magnetite-CCLS (c) maghemite-PCLS and maghemite-CCLS

band was related to the FTIR spectroscopy, as absorption peaks of Fe-O appear in the visible fingerprint region of 575-400 cm^{-1} [26]. The different broadening surface plasmon resonance indicates a polydispersive material which becomes slightly red shifted with increase in wavelength [59]. This suggests that if sucrose a non-reducing saccharide which acts as both a stabilizer for the inhabitation of agglomeration due to dipole-dipole attraction and solubilizer for biogenic calcium carbonate was not used larger aggregated nanocomposites would have formed [60].

Photoluminescence studies: The photoluminescence results are shown in Fig. 4. It was observed that the magnetic nanocomposites of maghemite exhibited both a red shift extreme 467 nm for maghemite-PCLS and 435 for maghemite-CCLS and blue shift 396 for both materials due to their size distribution. This could be attributed to the size distribution of the nanoparticles as observed on SEM, the polycrystalline nature of the surface of both materials was made up of both fine and coarse particles. Magnetite-PCLS exhibited a slight red shift which was attributed to Ostwald ripening effect whereby the nanoparticles tend to nucleate to form larger particles, this could be due to the longer mixing time during synthesis [61]. Magnetite however did not exhibit any red or blue shift, the excitation was representative of one of the absorption wavelengths exhibited by the material. The nanocomposite also exhibited a lower band gap 1.49, 1.68, 1.78 and 1.87 eV for maghemite-PCLS, magnetite-PCLS, maghemite-CCLS and magnetite-CCLS [62-64], the band gap was found to be comparable to that in literature. This lower energy band gap was indicative of the increase in size, which can be attributed to the use of PCLS and CCLS. However, it has also been reported that the colour of nanoparticles also plays a huge role in the lowered bandgap of materials [65]. Therefore, the colour of the materials which is an intense earthy red/brown for maghemite and black for magnetite could be attributed to the observed band gap.

$pH_{(PZC)}$ studies: The physico-chemical properties of $pH_{(PZC)}$ of the adsorbents were analyzed and the results are shown in Table-1. The surface charge density plays a big role during the process of adsorption because it determines interaction with the different species of solutes in the solution and affects the uptake of metals and their fate onto the surface of the materials. The dominating species at basic pH for iron oxide are $Fe(OH)_2^0$ and $Fe(OH)_3^-$ and at acidic pH the dominating species is Fe^{2+} and less dominating is $Fe(OH)^{2+}$ [66]. The surface of the magnetite samples was basic, while the surface of the

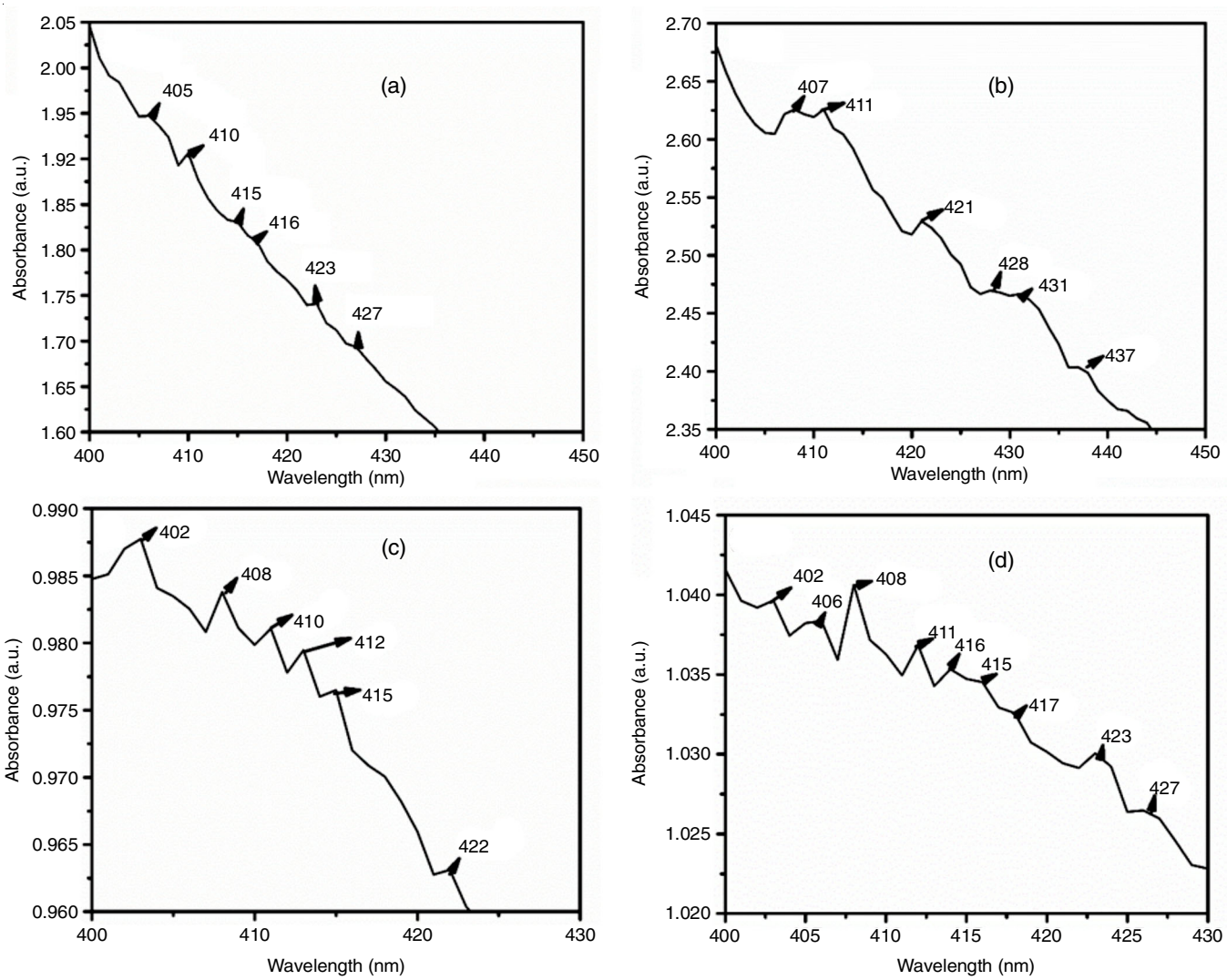

Fig. 3. UV/vis of (a) magnetite-PCLS (b) magnetite-CCLS (c) maghemite-PCLS and maghemite-CCLS

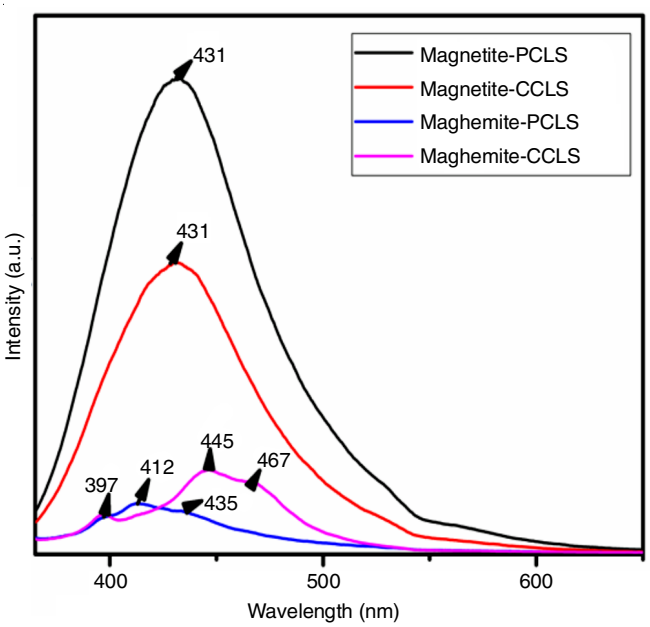

Fig. 4. Photoluminescence analysis of magnetite-PCLS, magnetite-CCLS, maghemite-PCLS and maghemite-CCLS

TABLE-1
$pH_{(PZC)}$ OF MAGNETITE-PCLS, MAGNETITE-CCLS, MAGHEMITE-PCLS AND MAGHEMITE-CCLS

$pH_{(PZC)}$	Magnetite-PCLS	Magnetite-CCLS	Maghemite-PCLS	Maghemite-CCLS
KNO_3	8.5	8.7	6.2	6.8

maghemite samples was in the acidic region. Below is the possible mechanism for the interactions of the metal with differently protonated and deprotonated surface of the adsorbents.

$Fe\text{-}OH + H^+ = Fe\text{-}OH_2^+$ possible mechanism of the surface protonation at $pH < pH_{(PZC)}$

$Fe\text{-}OH = Fe\text{-}O^- + H^+$ possible mechanism of the surface deprotonation at $pH > pH_{(PZC)}$

Adsorption data

Effect of time: The plot for effect of time is shown in Fig. 5a-b. The data reveals the trends for the uptake of Pb(II) and Cr(VI) onto the adsorbents. The rate of metal uptake was very rapid during the initial stage of adsorption (5-40 min), this was followed by a much slower rate from (60-120 min). Equilibrium was reached for magnetite-PCLS (Fig. 5a) for the

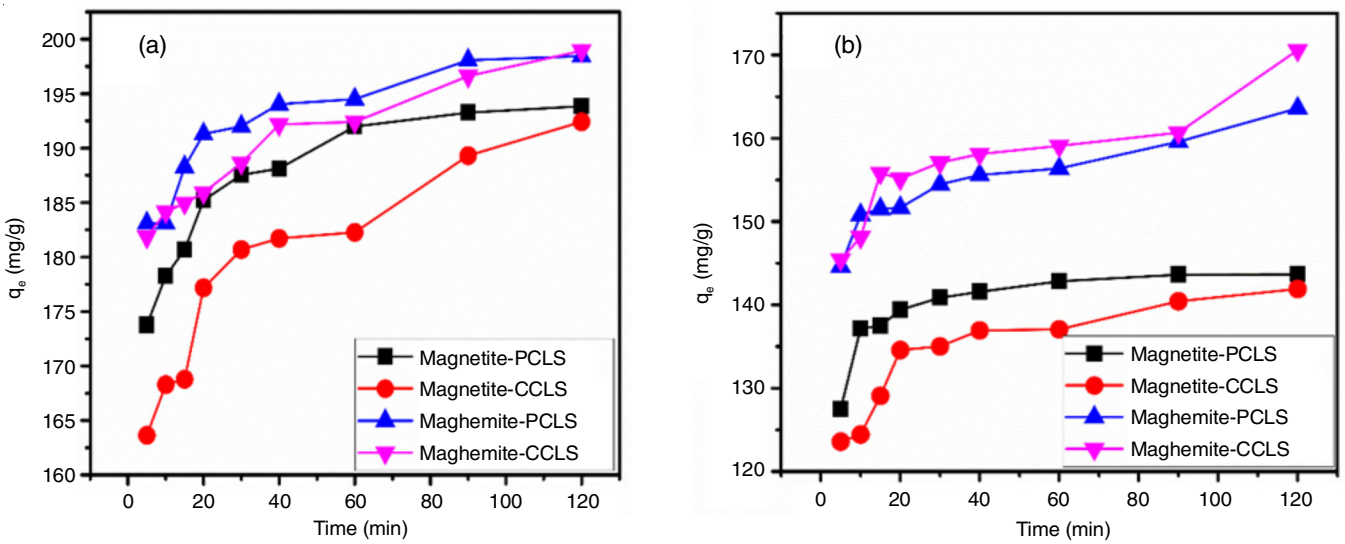

Fig. 5. Effect of time for adsorption of (a) Pb(II) and (b) Cr(VI)

uptake of Pb(II) and Fig. 5b shows the uptake of Cr(VI) within 60 min. However, uptake for the other adsorbents (magnetite-CCLS, maghemite-PCLS and maghemite-CCLS) for both adsorptions of Pb(II) and Cr(VI) displayed a continuous increase. The uptake trend for Pb(II) was maghemite-CCLS 198.94 mg/g > maghemite-PCLS 198.46 mg/g > magnetite-PCLS 193.85 mg/g > magnetite-CCLS 192.42 mg/g and for Cr(VI) maghemite-CCLS 170.59 mg/g > maghemite-PCLS 163.6 mg/g > magnetite-PCLS 143.66 mg/g > magnetite-CCLS 141.91 mg/g. The data suggests that maghemite had much reactivity towards the uptake of the metal ions. The rapid adsorption in the initial stages of adsorption is ascribed to the unoccupied spaces within the surface of the adsorbents and vacant pores which are actively interacting with the ions. From 60-120 min, the surface is fully saturated with the adsorbate, the solutes will therefore move to the internal sites of the pores. Hence, the slow metal uptake beyond 60 min is observed.

Kinetic studies: Kinetic studies were done to further probe the rate of adsorption of the solid-liquid interaction between the adsorbate and the adsorbent. The data was probed for the diffusion of solutes onto the surface of the adsorbent and further into the pore structure. The kinetic data describes the mechanism for adsorption of Cr(VI) and Pb(II) by the prepared adsorbents maghemite-CCLS, maghemite-PCLS, magnetite-PCLS and magnetite-CCLS, with the kinetic models alongside the effect of time data. The data showed that during the effect of initial time (0-30 min) the graph is superimposed onto data for all the adsorbents in Figs. 6a-d and 7a-d. However, with increase in time the PSO and IPD continue increasing as with the adsorption data. The PFO kinetic model reached equilibrium whereby it was observed that the graphs forms a sort of parallel line to the x-asymptote [67]. Hence, the correlation (r^2) for Cr(VI) adsorption of 0.60, 0.70 and 0.62 for magnetite-CCLS, maghemite-PCLS and maghemite-CCLS, respectively and for Pb(II) 0.61, 0.60 and 0.52 for magnetite-CCLS, maghemite-PCLS and maghemite-CCLS is observed. However, magnetite-PCLS adsorbent showed a superimposition on the PFO model (Figs. 6a and 7a), hence the correlation (r^2) for Pb(II) is 0.70 for magnetite-PCLS and 0.90 for Cr(VI) onto magnetite-PCLS (Table-2). The deviation in correlation for adsorption of Pb(II) and Cr(VI) onto magnetite-CCLS, maghemite-PCLS and maghemite-CCLS (Figs. 6b-d and 7b-d) has been attri-buted to findings, which suggests that generally the PFO model was usually a good fit for the initial stages of adsorption but does not represent the full adsorption data [68]. PSO better fitted the adsorption data with calculated q_e values that were closer to the experimental values for both metals. The time scaling factor K_2 was low with a large q_e proving that the adsorption data describing the system reached equilibrium much slower [69], this proved that PSO was not the only mechanism for adsorption and therefore not the rate limiting step and that adsorption was due to the synergetic adsorption mechanisms such as chemisorption (electrostatic interaction) and physisorption (pore-entrapment or diffusion). Hence the charge density of the nanocomposites on the surface was crucial because of the high affinity for uptake.

The mass transfer theory relates to the diffusion of solutes within the structure of the adsorbents [70]. This theory is described by the movement of the adsorbent from the bulk to the adsorbent surface whereby surface diffusion of surface adsorption can take place and further movement into the pore structure whereby intra-particle diffusion occurs. The plots of Pb(II) and Cr(VI) for IPD model of magnetite-PCLS, magnetite-CCLS, maghemite-PCLS and maghemite-CCLS were defined by two stages, namely surface diffusion and pore diffusion [71]. For surface diffusion at 5-40 min, the rate at which the adsorbent diffused onto the surface of the adsorbent was rapid due to the free binding sites on the surface. The adsorption was rapid at initial stages, therefore this suggested that the surface adsorption was the rate limiting step, however it was not the only mechanism of adsorption which took place. Pore diffusion at 60 to 120 min described the movement of the adsorbate to the pore structure of the adsorbent whereby the solute was retained and intraparticle diffusion also occurred. The increasing linear nature of the IPD graph from 60 to 120 min of adsorption suggested that further diffusion of the adsorbate towards the

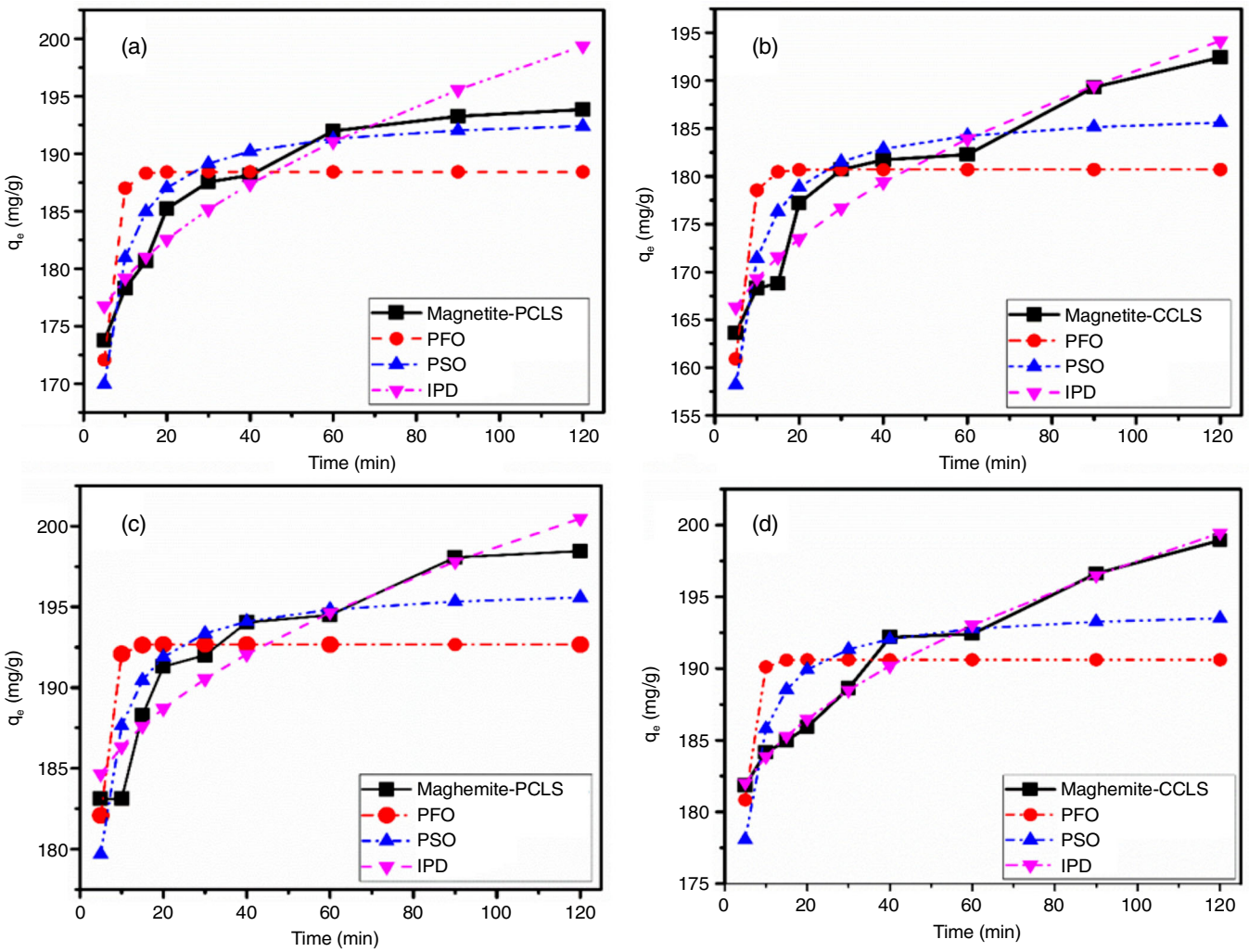

Fig. 6. Kinetic data for adsorption of Pb(II) onto (a) magnetite-PCLS (b) magnetite-CCLS (c) maghemite-PCLS and maghemite-CCLS

TABLE-2
KINETICS PARAMETERS AND MODELLING DATA

Isotherm	Parameter	Magnetite-PCLS		Magnetite-CCLS		Maghemite-PCLS		Maghemite-CCLS	
		Pb(II)	Cr(VI)	Pb(II)	Cr(VI)	Pb(II)	Cr(VI)	Pb(II)	Cr(VI)
PFOM	q_e (mg/g)	188.43	141.09	180.71	134.14	192.67	155.64	190.62	158.37
	K_1	0.489	0.46	0.44	0.48	0.58	0.52	0.594	0.48
	r^2	0.643	0.91	0.613	0.59	0.582	0.72	0.524	0.62
PSOM	q_e (mg/g)	193.52	144.22	187.02	138.1	196.34	159	194.24	162.76
	K_2	0.01	0.011	0.005	0.01	0.0011	0.011	0.011	0.01
	r^2	0.902	0.99	0.883	0.87	0.89	0.88	0.822	0.90
IPD	q_e (mg/g)	170.97	130.99	159.21	120.5	180.59	143.53	177.54	142.8
	K_i	2.59	1.4	3.19	2.07	1.82	1.8	2.01	2.31
	r^2	0.97	0.81	0.96	0.96	0.94	0.96	0.99	0.94
EPA	%	11.8	8.86	17.26	15.09	9	12.27	10.76	16.29
ESA	%	88.19	91.24	82.76	84.91	90.09	87.73	89.24	83.71
Experimental	q_e (mg/g)	193.85	143.66	192.42	141.91	198.46	163.6	198.94	170.59

%EPA-Estimated pore adsorption; %ESA-Estimated surface adsorption

pores of the adsorbents was also a defining mechanism for the uptake of metals, however it was not the rate limiting step.

Effect of concentration: The effect of solution concentration for Pb(II) and Cr(VI) was evaluated at concentration range 20-200 mg/L. From the plots (Fig. 8a-b), it was observed that the adsorption increased with the increase in concentration. Therefore mass transfer was observed for higher concentration solutions [72], this can be attributed to the hindering forces which were overcome. At low concentrations the solutes become saturated onto the surface of the adsorbents, the saturated surface of the adsorbents will then prompt movement of solutes onto the internal surface leading to higher adsorption capacity [73].

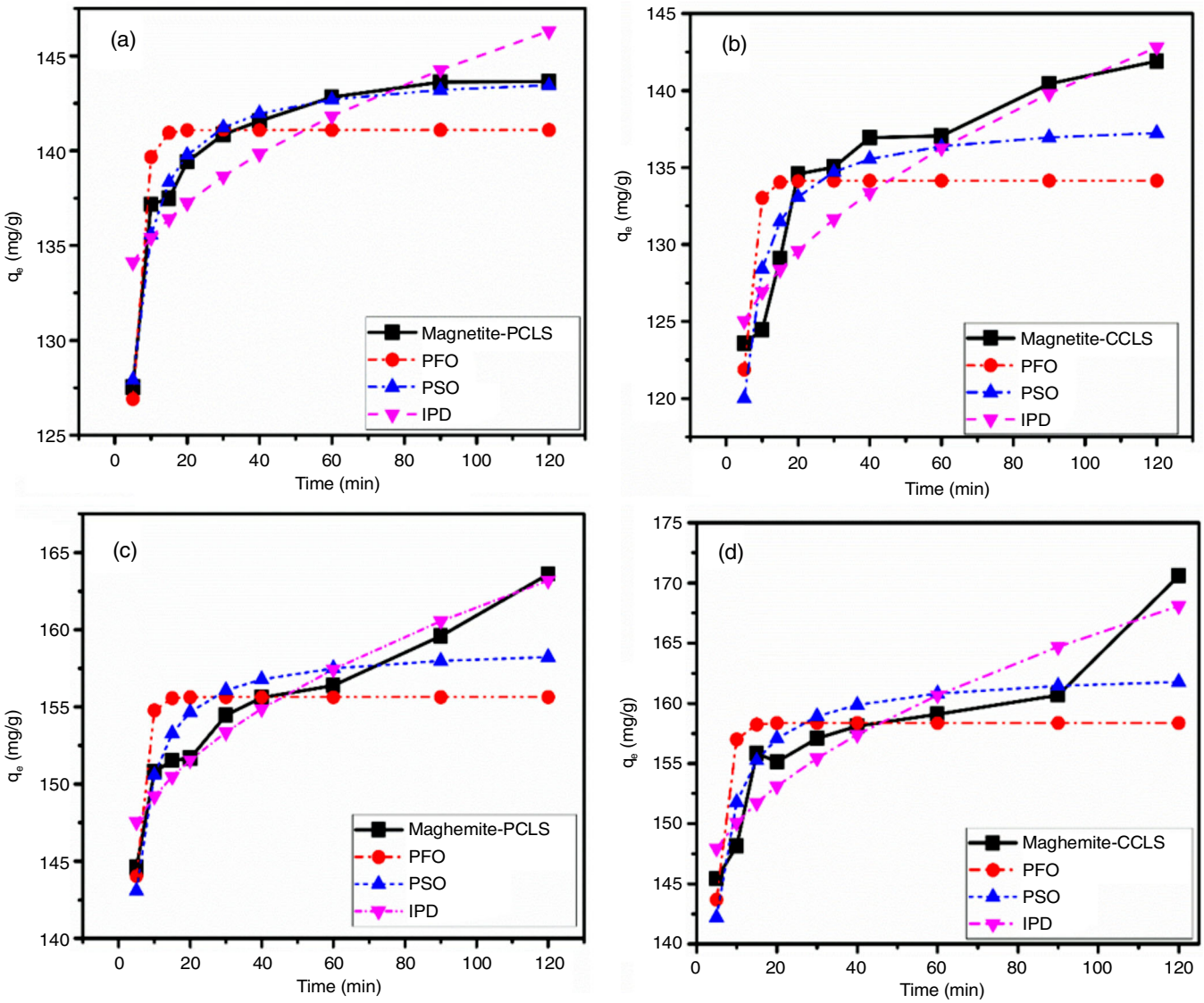

Fig. 7. Kinetic data for adsorption of Cr(VI) onto (a) magnetite-PCLS (b) magnetite-CCLS (c) maghemite-PCLS and maghemite-CCLS

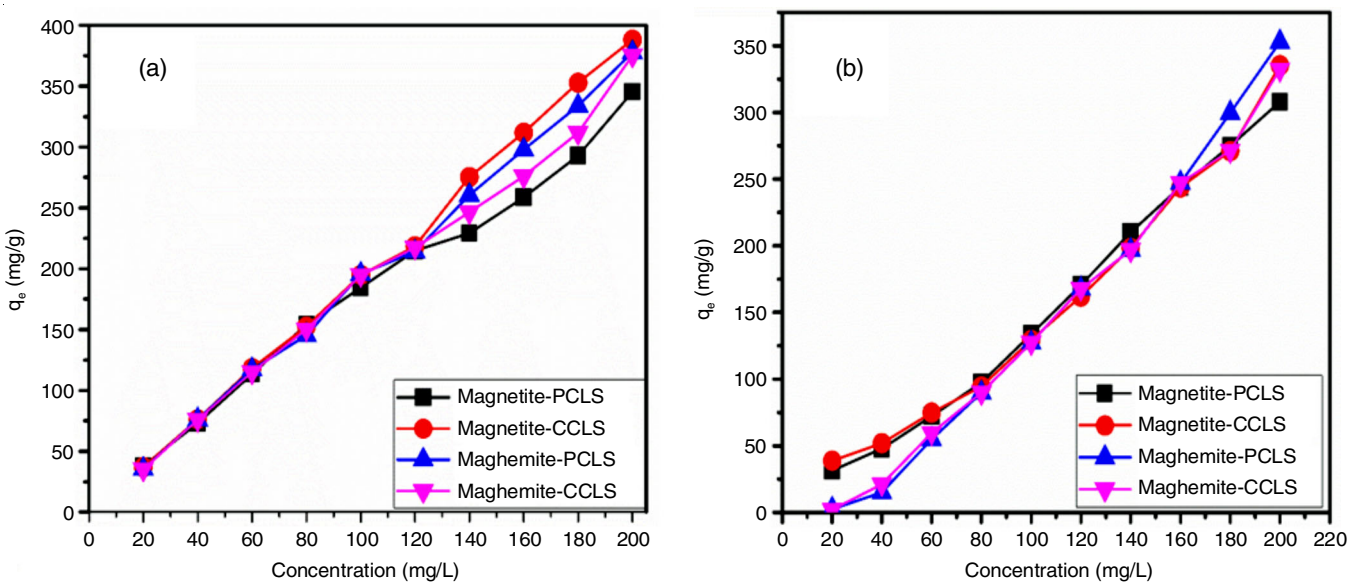

Fig. 8. Effect of concentration of (a) Pb(II) and (b) Cr(VI)

Adsorption isotherms: The adsorption of Pb(II) and Cr(VI) onto the surface of the adsorbents was integrated into Langmuir, Freundlich and Dubinin-Radushkevich models to further understand the removal mechanisms. Langmuir assumes that an adsorbent surface is homogenous [74], hence the energy distribution is constant. The adsorbed species therefore forms a monolayer of which the sites of adsorption on the adsorbate are independent of the next and have an affinity towards the adsorbate. The adsorption data (Table-3) was found to poorly fit Langmuir isotherm, the parameter β was very low for Cr(VI) onto magnetite-PCLS, magnetite-CCLS, maghemite-PCLS and maghemite-CCLS and for Pb(II) onto magnetite-CCLS and maghemite-PCLS suggested that the adsorbent surface was dominated by sites, which did not have an affinity for the adsorbate. However, adsorption of Pb(II) onto magnetite-PCLS and maghemite-CCLS better fitted Langmuir compared to all the other adsorbents, this can be attributed to the higher surface affinity toward Pb(II). Furthermore, the data was fitted onto Freundlich isotherm which suggests a heterogeneous surface [75], of which the adsorption of molecules follows a multilayer mechanism. It is important to note that the distribution of the adsorbate onto the surface binding sites was singular, hence the model suggested that the binding sites on the adsorbate surface are grouped according to their energy [68]. This instance makes for the provision of the faster binding sites to have a strong affinity of the solutes in solution. From the adsorption data, it was observed that Freundlich model was a better fit compared to Langmuir isotherm model for the adsorbents. The correlation of as-synthesized nanocomposites for the Freundlich isotherm was between 0.840-0.965 suggested that the surface of the adsorbent is heterogeneous and multilayer adsorption is possible. The surface heterogeneity factor measures the intensity at which the adsorbate stuck to the active binding sites on the heterogeneous adsorbate suggested that adsorption was favourable [76].

The tendency of the data to become favourable towards adsorption suggested that the data could be explained further to understand the mechanism of adsorption. Therefore, the data was further investigated using the Dubinin-Radushkevich isotherm model, which accounts for pore filling onto the surface of the adsorbent [75]. The model is related to the adsorption potential theory which accounts for the adsorbate mechanism by pore filling. The adsorption potential theory accounts for the change in Gibbs free energy of an adsorbate after it stuck to the binding site of the adsorbent. Thus, the model can predict the adsorption process from mean free energy (E). The mean free energy value of the D-R isotherm suggested that when (E) < 8, the mechanism is physisorption [77,78].

Effect of temperature: The effect of temperature was evaluated at different concentrations 20-100 mg/L at 288, 298 and 308 K to understand the uptake of the adsorbate onto the adsorbents, when temperature is introduced into the system. It has been observed that an increase in the energy of the system may course either an increase in the uptake of the adsorbate or a decrease. It was observed that for both maghemite samples, maghemite-PCLS and maghemite-CCLS, an increase in the temperature supplied enough energy to the system for higher uptake, however the increase was not significantly high (Fig. 9c-d). However, at high temperature 309 K, the uptake was lower compared to at 288 K. This leads to the assumption that the uptake of Pb(II) onto the maghemite is not temperature dependant as higher uptake is observed for the temperature 288 K for all the samples.

An increase in temperature from 289 to 299 K was not significant for the uptake of Cr(VI) by magnetite-PCLS and magnetite-CCLS (Fig. 10a-b). However, further increase to 309 K an increase in the uptake of Cr(VI) with magnetite-CCLS significantly showing a higher uptake as compared to 289 K. This trend was however not observed for the adsorption of maghemite samples (Fig. 10c-d), where increase into the system energy decreased the uptake of the pollutant.

Thermodynamic studies: The adsorption data were subjected to thermodynamic studies (Table-4) to understand the temperature dependency of the adsorbents in relation to pollutant uptake. It was observed that when temperature was increased the adsorption resulted in an endothermic reaction for the uptake of Pb(II) for magnetite (magnetite-PCLS and magnetite-CCLS) and maghemite (maghemite-PCLS and maghemite-CCLS) for the uptake of Cr(VI). This was attributed by the lower values of entropy (ΔSº), which indicate an increased degree of freedom and random movements of the molecules in solution and the higher values of (ΔHº) [79]. The metal uptake increased with an increase in temperature, hence a higher uptake was observed due to the energy received

TABLE-3
ISOTHERM MODELLING OF ADSORPTION DATA

Isotherm	Parameter	Magnetite-PCLS		Magnetite-CCLS		Maghemite-PCLS		Maghemite-CCLS	
		Pb(II)	Cr(VI)	Pb(II)	Cr(VI)	Pb(II)	Cr(VI)	Pb(II)	Cr(VI)
Langmuir	Q_o (mg/g)	555.6	63.29	5.77	3.53	151.52	26.18	1.196	37.19
	β	0.18	2.12×10^{-3}	0.00614	5.87×10^{-3}	1.24×10^{-4}	0.021	0.0204	6.35×10^{-3}
	r^2	0.930	0.0021	0.580	0.572	0.711	0.660	0.580	0.874
Freundlich	K_f	99.88	4.40×10^{-8}	92.18	2.85×10^{-8}	100.44	0.888	0.014	10.73
	n	1.941	0.154	1.867	0.1502	2.91	5.12	1.24	1.09
	r^2	0.963	0.905	0.937	0.875	0.934	0.957	0.841	0.941
Dubinin Radushkevich	qs	757.02	0.904	1.59	0.877	744.1	0.885	27.46	0.883
	Kdr	1.36	1.37	0.406	1.49	1.41	1.386	0.401	1.434
	E	0.825	0.828	2.28	0.863	0.839	0.601	0.447	0.5901
	r^2	0.996	0.993	0.991	0.988	0.996	0.994	0.9801	0.993
Experimental	q_e (mg/g)	345.34	308.01	388.31	335.3	377.92	3352.91	375.35	335.27

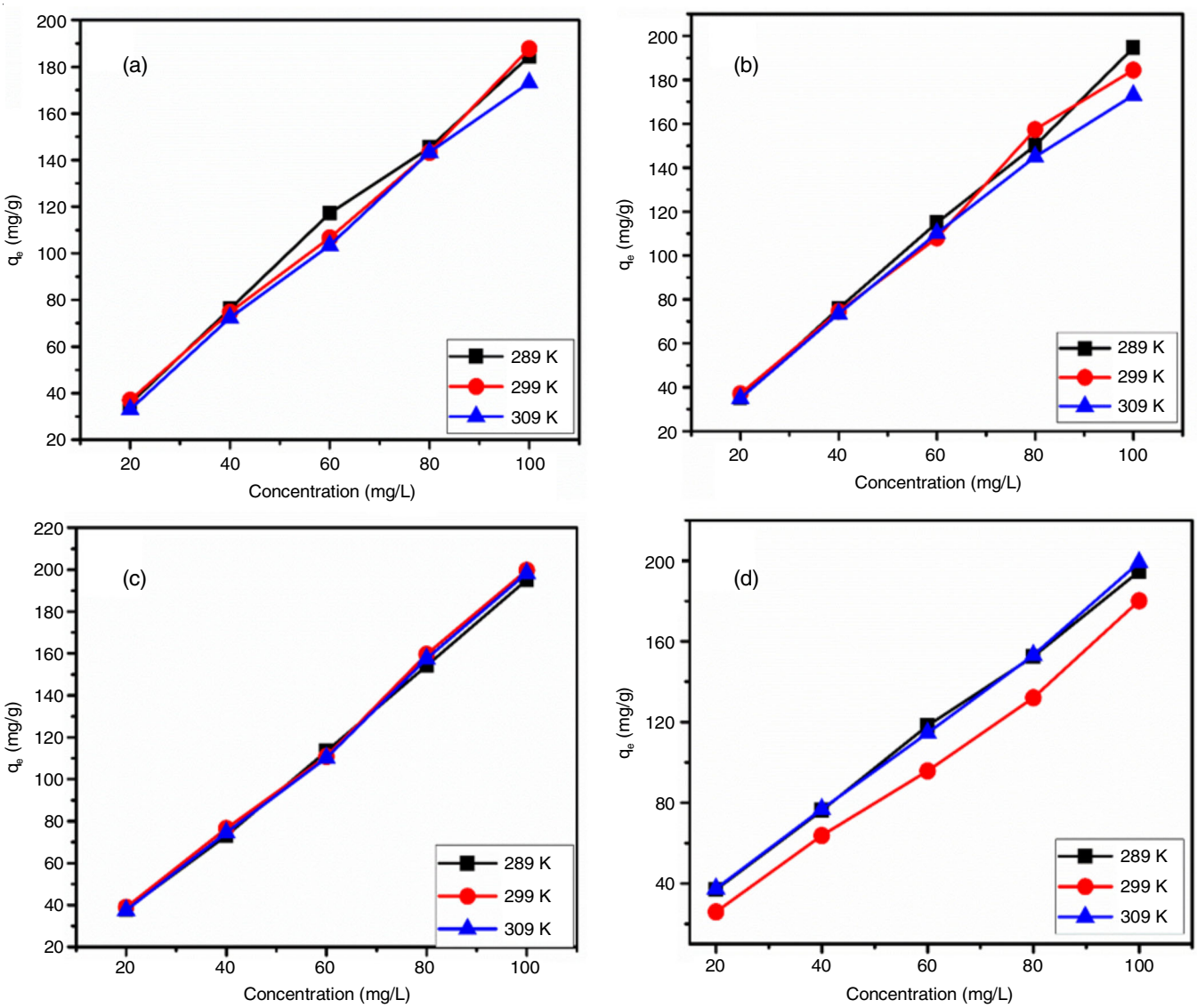

Fig. 9. Effect of temperature for (a) magnetite-PCLS, (b) magnetite-CCLS, (c) maghemite-PCLS and (d) maghemite-CCLS for the adsorption of Pb(II)

TABLE-4
THERMODYNAMIC STUDIES OF ADSORPTION DATA

Isotherm	Parameter	Magnetite-PCLS		Magnetite-CCLS		Maghemite-PCLS		Maghemite-CCLS	
		Pb(II)	Cr(VI)	Pb(II)	Cr(VI)	Pb(II)	Cr(VI)	Pb(II)	Cr(VI)
ΔH (KJ/mol)		6.17	-0.691	3.8	-3.32	-5.06	4.42	-2.23	4.53
ΔS (J/molK)		-16.9	3.84	-8.69	12.9	22.7	-13.1	12.5	-14.4
ΔG (KJ/mol)	289 K	-10.6	-3.62	-10.3	-3.72	-10.6	-5.65	-13.6	-6.12
	299 K	-8.623	-3.37	-10.6	-3.49	-17.9	-3.58	-7.54	-3.38
	399 K	-7.32	-3.99	-8.21	-5.54	-13.2	-3.29	-14.91	-3.56

by the adsorbate [79]. The observed tendency was opposite for magnetite uptake of Cr(VI) on (magnetite-PCLS and CCLS) and maghemite (maghemite-PCLS and CCLS) for the uptake of Pb(II). The negative values of enthalpy (ΔH^o) described an exothermic system which was attributed to the higher values of entropy (ΔS^o) [80]. Thus, when the temperature is increased the adsorbents release energy hence an increase in temperature will result in a lower uptake. The adsorption process is an indicative of a decreased degree of freedom and random movement of the molecules in solution. The overall adsorption process was spontaneous and favourable which is supported by the negative values of Gibb's free energy for the system.

Effect of pH: The effect of pH was studied at pH 2, 4, 6 8 and 10 for Cr(VI) and pH 2, 4, 6 and 8 for Pb(II). It was observed that the uptake of both Pb(II) and Cr(VI) is pH dependant due to the chemical species which exist at each pH maxima and minima (Fig. 11). In acidic solutions where pH < 6.5 the predominant species are Pb(II) and $Pb(OH)^+$ and at

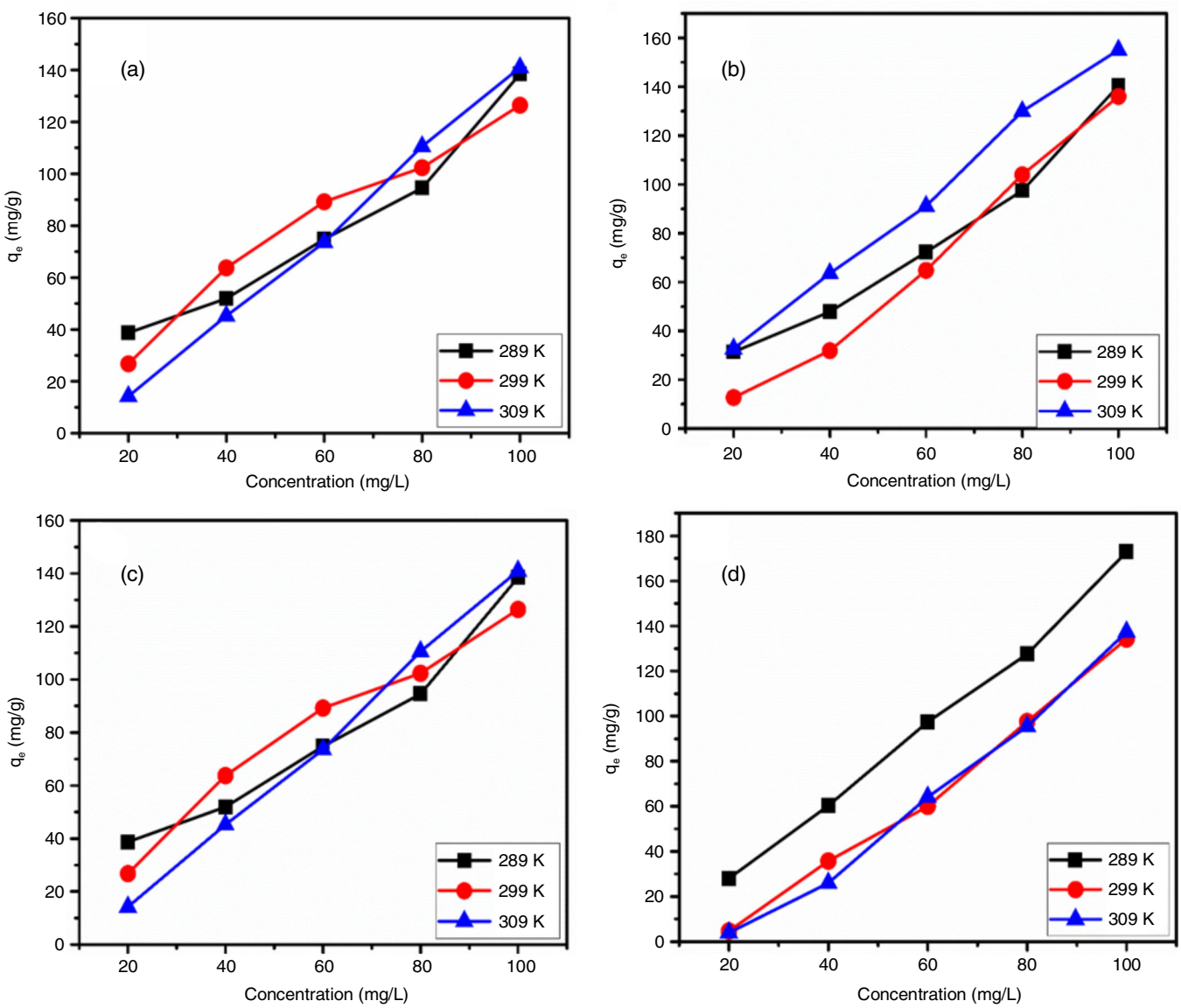

Fig. 10. Effect of temperature for (a) magnetite-PCLS, (b) magnetite-CCLS, (c) maghemite-PCLS and (d) maghemite-CCLS for the adsorption of Cr(VI)

higher pH > 6.5 $Pb(OH)_2$ predominates [11]. Due to the competition which exists between the cations and the protonated surface, it is expected that repulsion would occur thus a lower uptake of lead would be observed in acidic conditions [81]. However, iron oxide (γ-Fe_2O_3 and Fe_3O_4) was observed to be an amphiprotic oxide [82], this therefore meant that at lower pH some FeO^- can be found on the surface although the dominating species are Pb(II) and $Pb(OH)^+$. The uptake of Pb(II) by the adsorbents as reported was below the $pH_{(PZC)}$, this therefore meant that the presence of $Fe(OH)_3^-$ was responsible for the metal uptake Cr(VI) exists as oxy-ions of hydrochromate ($HCrO_4^-$), which is found at pH 0-2, dichromate ($Cr_2O_7^{2-}$) dominating at pH 2-6 and lastly chromate (CrO_4^{2-}) at pH 7-14 [83]. The nanocomposites adsorbents were observed to have good adsorption in the region 2-6 whereby hydrochromate and dichromate are more dominative in neutral solution. When the pH is further increased to alkaline conditions the surface of the nanocomposites would be deprotonated thus adsorption would decrease [84], however it is observed that uptake increases for Cr(VI) onto maghemite-CCLS, magnetite-PCLS and magnetite-CCLS. The uptake of chromate (CrO_4^{2-}) at pH 10 was distinctive to the nature of the material surface charge density as iron oxide is an amphiprotic oxide, hence at pH 7-14, $Fe(OH)_3^-$ and $Fe(OH)_2^0$ would repel chromate. However, uptake was due to the less dominating species of iron oxide $Fe(OH)_3^-$ and $Fe(OH)^{2+}$.

Comparative study: A comparative study (Table-5) was done to show the comparison of the effectiveness of the studied adsorbents for removal of the metals with reported adsorbents.

Regeneration studies: Regeneration and reusability test of the adsorbents was evaluated and the results are shown in Fig. 12. The regenerative were done by using 10 mg of the adsorbents in 20 mL of the solution containing pollutants at 10 ppm for 120 min. The adsorbents were then washed with 0.001 M HCl solution. It was observed that the adsorbents were able to regenerated up to 3 cycles. The uptake of the toxic metals

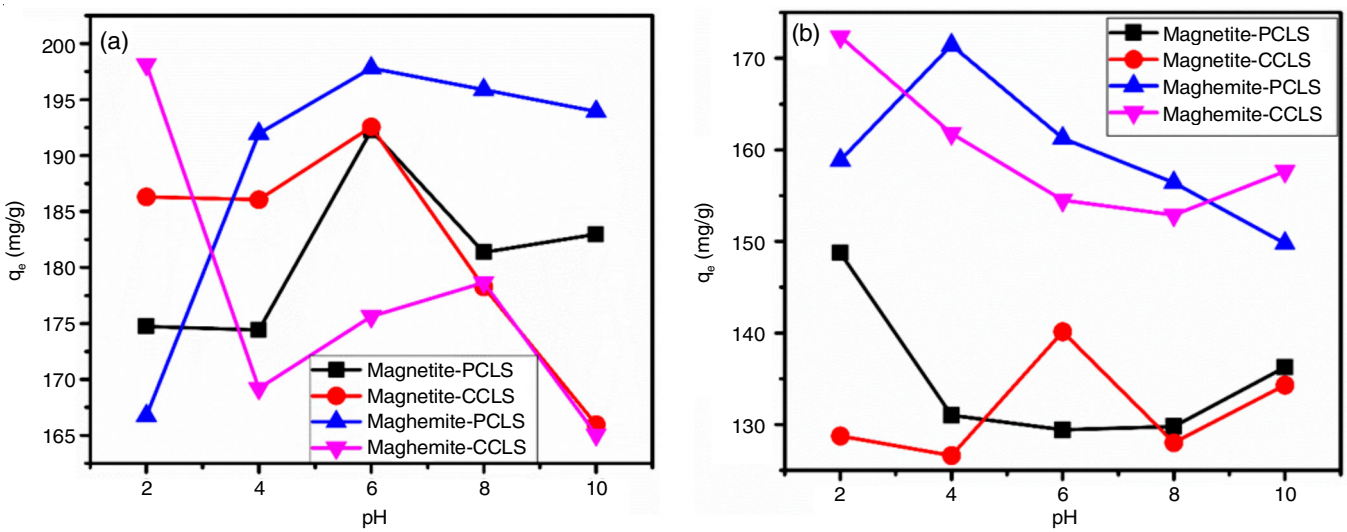

Fig. 11. Effect of solution pH of (a) Pb(II) and (b) Cr(VI)

TABLE-5
COMPARATIVE STUDY

Adsorbent name	Pollutant	Adsorbent mass	q_e (mg/g)	Initial concentration	Removal (%)	Ref.
Magnetite-PCLS	Cr(VI)	10 mg	143.66	100 ppm	71.8	This study
Magnetite-CCLS	Cr(VI)	10 mg	141.91	100 ppm	70.8	This study
Maghemite-PCLS	Cr(VI)	10 mg	163.60	100 ppm	81.8	This study
Maghemite-CCLS	Cr(VI)	10 mg	170.59	100 ppm	86.2	This study
γ-Fe_2O_3	Cr(VI)	5 g/L	–	50 ppm	97.3	[12]
γ-Fe_2O_3	Cr(VI)	5 g/L	–	100 ppm	74.6	[12]
γ-Fe_2O_3	Cr(VI)	5 g/L	–	150 ppm	58.9	[12]
Magnetite-PCLS	Pb(II)	10 mg	198.94	100 ppm	99.8	This study
Magnetite-CCLS	Pb(II)	10 mg	198.46	100 ppm	99.1	This study
Maghemite-PCLS	Pb(II)	10 mg	192.42	100 ppm	99.2	This study
Maghemite-CCLS	Pb(II)	10 mg	193.83	100 ppm	99.5	This study
Fe_3O_4	Pb(II)	20 mg/L	–	50 ppm	100	[85]
m-PAA-na	Pb(II)	1 g	40 mg/g	18 ± 1 ppm	–	[86]
T-Fe_2O_3	Pb(II)	0.6 g/L	15.81	10 ppm	–	[87]
T-Fe_2O_3	Pb(II)	0.6 g/L	31.57	20 ppm	–	[87]

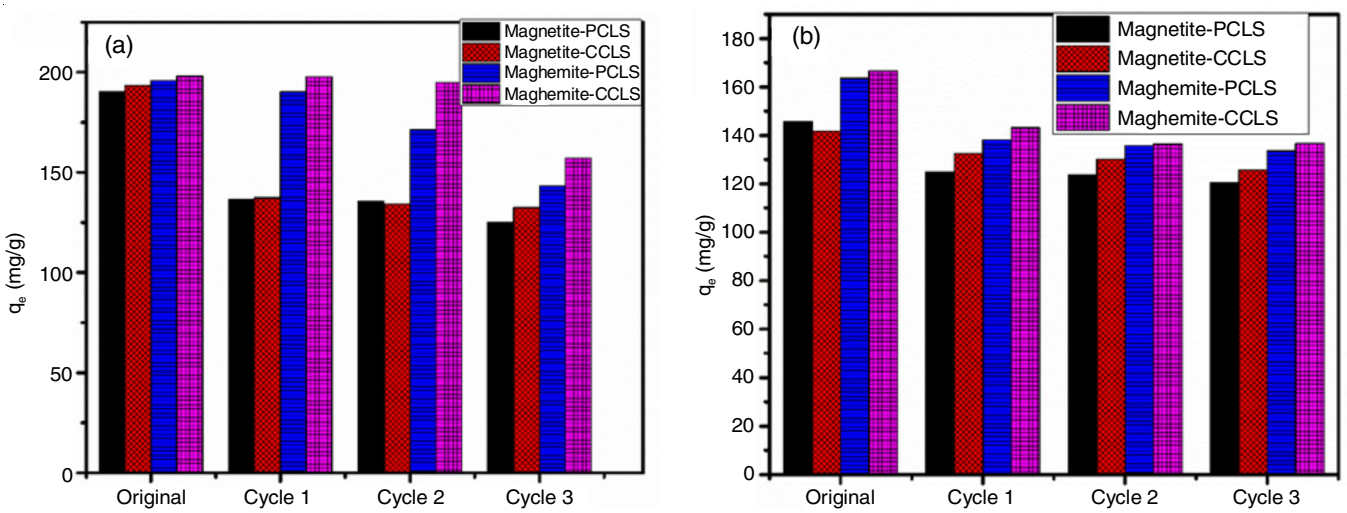

Fig. 12. Regenerative studies of the adsorbents for the uptake of (a) Pb(II) and (b) Cr(VI)

was initially high, which can be expected due to the unoccupied surface pores and active functional groups on the surface of the materials. Due to the nature of metal uptake in terms of mechanism of uptake, it was observed that a combination of physical, chemical and pore adsorption was observed in kinetics and isotherm modelling. The role of the surface charge density

was also important because of the active functional groups which influenced uptake. Hence, it was observed that the detachment of the metal ions was difficult due to electrostatic bonding, the encountered desorption was attributed to pore desorption. As observed in kinetics, pore adsorption was not the rate determining step. Surface desorption of Pb(II) and Cr(VI) was difficult due to the electrostatic attractions between the initially adsorbed metal ions and surface functionalities. Hence, upon each subsequent cycle less adsorption occurs, however better reusability of maghemite was observed compared to magnetite.

Conclusion

The synthesis of magnetic nanocomposites for magnetite and maghemite using co-precipitation was successful. This was proved by the FTIR with a characteristic peak of Fe-O in the visible region from 400-500 cm^{-1}. The UV/visible analysis also confirmed the formation of the iron oxide nanocomposites with excitation in the visible region, which was found to be typical of the formation of the magnetic nanocomposites. The SEM spectroscopy confirmed the formation of the nanocomposites with a variation in the surface distribution and deviation from sphericity, the nanocomposites were also amorphous. The physico-chemical properties showed that the surface of the magnetite samples were basic, while maghemite were acidic. Adsorption was successfully carried out by varying parameters such as time, concentration, temperature and pH. From these parameters, it was observed that adsorption was defined better by multilayer adsorption. Furthermore the data was fit onto the D-R isotherm, the E parameter was below 8 KJ/mol, which suggested the physical adsorption. From the kinetic data it was observed that the rate determining step was surface adsorption in intraparticle diffusion, this was also supported by the better fitting of the pseudo-second order model suggested the adsorption was initially rapid due to the chemical adsorption onto the active functional groups present on the material surface. It was also observed that pore adsorption played a role in the adsorption process, hence the obtained data for kinetic studies in combination with isotherm modelling suggested both physical and chemical adsorption was possible. Therefore, the overall data suggests that the new adsorbents *viz*. magnetite-PCLS, magnetite-CCLS, maghemite-PCLS and maghemite-CCLS can be possibly be applied to water and wastewater treatment.

ACKNOWLEDGEMENTS

Support for this research was provided by the National Research Fund (NRF) of South Africa (Grant: TTK19040342-6819) and the Vaal University of Technology, Vanderbijlpark, South Africa.

CONFLICT OF INTEREST

The authors declare that there is no conflict of interests regarding the publication of this article.

REFERENCES

1. S.M. Bassem, *Biodiversity Int J.*, **4**, 10 (2020); https://doi.org/10.15406/bij.2020.04.00159
2. P.N. Diagboya, H.K. Mmako, E.D. Dikio and F.M. Mtunzi, *J. Environ. Chem. Eng.*, **7**, 103461 (2019); https://doi.org/10.1016/j.jece.2019.103461
3. H. Ali, E. Khan and I. Ilahi, *J. Chem.*, **2019**, 6730305 (2019); https://doi.org/10.1155/2019/6730305
4. M.O. Fashola, V.M. Ngole-Jeme and O.O. Babalola, *Int. J. Environ. Res. Public Health*, **13**, 1047 (2016); https://doi.org/10.3390/ijerph13111047
5. M.G.J. Hartl, eds.: C.M. Wood, A.P. Farrell and C.J. Brauner, Homeostasis and Toxicology of Non-Essential Metals, Elsevier: London, U.K. (2012).
6. N.D. Shooto, E.D. Dikio, D. Wankasi and L.M. Sikhwivhilu, *Hem. Ind.*, **71**, 221 (2017); https://doi.org/10.2298/HEMIND160120032S
7. M.W. Yap, N.M. Mubarak, J.N. Sahu and E.C. Abdullah, *J. Ind. Eng. Chem.*, **45**, 287 (2017); https://doi.org/10.1016/j.jiec.2016.09.036
8. P. Wang, T. Shen, X. Li, Y. Tang and Y. Li, *ACS Appl. Nano Mater.*, **3**, 1272 (2020); https://doi.org/10.1021/acsanm.9b02036
9. M. Eloussaief and M. Benzina, *J. Hazard. Mater.*, **178**, 753 (2010); https://doi.org/10.1016/j.jhazmat.2010.02.004
10. H.A. Aziz, M.N. Adlan and K.S. Ariffin, *Bioresour. Technol.*, **99**, 1578 (2008); https://doi.org/10.1016/j.biortech.2007.04.007
11. S. Rajput, L.P. Singh, C.U. Pittman Jr. and D. Mohan, *J. Colloid Interface Sci.*, **492**, 176 (2017); https://doi.org/10.1016/j.jcis.2016.11.095
12. J. Hu, G. Chen and I.M.C. Lo, *Water Res.*, **39**, 4528 (2005); https://doi.org/10.1016/j.watres.2005.05.051
13. A.D. Apte, V. Tare and P. Bose, *J. Hazard. Mater.*, **128**, 164 (2006); https://doi.org/10.1016/j.jhazmat.2005.07.057
14. C.S. Nkutha, P.N. Diagboya, F.M. Mtunzi and E.D. Dikio, *Water Environ. Res.*, **92**, 1070 (2020); https://doi.org/10.1002/wer.1303
15. H.-J. Lunk, *ChemTexts*, **1**, 6 (2015); https://doi.org/10.1007/s40828-015-0007-z
16. A. Godelitsas, J.M. Astilleros, K. Hallam, S. Harissopoulos and A. Putnis, *Environ. Sci. Technol.*, **37**, 3351 (2003); https://doi.org/10.1021/es020238i
17. J. Karpinska and U. Kotowska, *Water*, **11**, 2017 (2019); https://doi.org/10.3390/w11102017
18. D. Alidoust, M. Kawahigashi, S. Yoshizawa, H. Sumida and M. Watanabe, *J. Environ. Manage.*, **150**, 103 (2015); https://doi.org/10.1016/j.jenvman.2014.10.032
19. J. Hu, G. Chen and I.M.C. Lo, *J. Environ. Eng.*, **132**, 709 (2006); https://doi.org/10.1061/(ASCE)0733-9372(2006)132:7(709)
20. D.D. Do, Adsorption Analysis: Equilibria and Kinetics, Imperial College Press, vol. 2 (1998).
21. N. D. Shooto, P. M. Thabede, and E. B. Naidoo, *South African J. Chem. Eng.*, 30, 15 (2019); https://doi.org/10.1016/j.sajce.2019.07.002
22. A. Demirbas, *Energy Convers. Manage.*, **42**, 1357 (2001); https://doi.org/10.1016/S0196-8904(00)00137-0
23. N. Sarkar, S.K. Ghosh, S. Bannerjee and K. Aikat, *Renew. Energy*, **37**, 19 (2012); https://doi.org/10.1016/j.renene.2011.06.045
24. P. Panneerselvam, N. Morad and K.A. Tan, *J. Hazard. Mater.*, **186**, 160 (2011); https://doi.org/10.1016/j.jhazmat.2010.10.102
25. V. Patsula, M. Moskvin, S. Dutz and D. Horák, *J. Phys. Chem. Solids*, **88**, 24 (2016); https://doi.org/10.1016/j.jpcs.2015.09.008
26. Y.P. Yew, K. Shameli, M. Miyake, N. Kuwano, N. Bahiyah and B. Ahmad, *Nanoscale Res. Lett.*, (2016); https://doi.org/10.1186/s11671-016-1498-2
27. S. Mullerova, E. Baldikova, J. Prochazkova, K. Pospiskova and I. Safarik, *Mater. Chem. Phys.*, **225**, 174 (2019); https://doi.org/10.1016/j.matchemphys.2018.12.074
28. M.T. Hossain, M.M. Hossain, M.H.A. Begum, M. Shahjahan, M.M. Islam and B. Saha, *Bangladesh J. Sci. Ind. Res.*, **53**, 219 (2018); https://doi.org/10.3329/bjsir.v53i3.38269
29. F. Yazdani and M. Seddigh, *Mater. Chem. Phys.*, **184**, 318 (2016); https://doi.org/10.1016/j.matchemphys.2016.09.058

30. T. Tsuzuki and P.G. McCormick, *Acta Mater.*, **48**, 2795 (2000); https://doi.org/10.1016/S1359-6454(00)00100-2
31. K. Boustani, A. Shokri, S.F. Shayesteh and A. Jafari, *J. Supercond. Nov. Magn.*, **33**, 1879 (2020); https://doi.org/10.1007/s10948-020-05436-y
32. J.K. Oh and J.M. Park, *Prog. Polym. Sci.*, **36**, 168 (2011); https://doi.org/10.1016/j.progpolymsci.2010.08.005
33. M. Mikhaylova, D.K. Kim, N. Bobrysheva, M. Osmolowsky, V. Semenov, T. Tsakalakos and M. Muhammed, *Langmuir*, **20**, 2472 (2004); https://doi.org/10.1021/la035648e
34. W.S. Peternele, V. Monge Fuentes, M.L. Fascineli, J. Rodrigues da Silva, R.C. Silva, C.M. Lucci and R. Bentes de Azevedo, *J. Nanomater.*, **2014**, 1 (2014); https://doi.org/10.1155/2014/682985
35. L. Mohammed, H.G. Gomaa, D. Ragab and J. Zhu, *Particuology*, **30**, 1 (2017); https://doi.org/10.1016/j.partic.2016.06.001
36. X. Sun, C. Zheng, F. Zhang, Y. Yang, G. Wu, A. Yu and N. Guan, *J. Phys. Chem. C*, **113**, 16002 (2009); https://doi.org/10.1021/jp9038682
37. A. Hajdú, E. Illés, E. Tombácz and I. Borbáth, *Colloids Surf. A Physicochem. Eng. Asp.*, **347**, 104 (2009); https://doi.org/10.1016/j.colsurfa.2008.12.039
38. Atul, M. Kumar, A. Sharma, I.K. Maurya, A. Thakur and S. Kumar, *J. Taibah Univ. Sci.*, **13**, 280 (2019); https://doi.org/10.1080/16583655.2019.1565437
39. A. Lim and A. Aris, *Rev. Environ. Sci. Biotechnol.*, **13**, 163 (2014); https://doi.org/10.1007/s11157-013-9330-2
40. E. Tombácz, A. Majzik, ZS. Horvát and E. Illés, *Rom. Rep. Phys.*, **58**, 281 (2006).
41. C. Su, *J. Hazard. Mater.*, **322**, 48 (2017); https://doi.org/10.1016/j.jhazmat.2016.06.060
42. M. Aghazadeh, I. Karimzadeh, M.R. Ganjali and M.M. Morad, *Mater. Lett.*, **196**, 392 (2017); https://doi.org/10.1016/j.matlet.2017.03.064
43. L.P. Hoang, T.M.P. Nguyen, H.T. Van, T.K.D. Hoang, X.H. Vu, T.V. Nguyen and N.X. Ca, *Water Air Soil Pollut.*, **231**, 28 (2020); https://doi.org/10.1007/s11270-020-4406-4
44. M.T. Samadi, R. Nourozi, M.H. Mehdinejad and R. Aminzadeh, *Iran. J. Health Environ.*, **5**, 479 (2013).
45. R. Shokohi, H.R. Ehsani and M. Tarlani Azar, *J. Environ. Sci. Technol.*, **16**, 109 (2014).
46. M. Malakootian, S. Mohammadi, N. Amirmahani, Z. Nasiri and A. Nasiri, *J. Commun. Health Res.*, **5**, 73 (2016).
47. C.S. Nkutha, N.D. Shooto and E.B. Naidoo, *South African J. Chem. Eng*, **34**, 151 (2020); https://doi.org/10.1016/j.sajce.2020.08.003
48. C.S. Nkutha, N.D. Shooto and E.B. Naidoo, *Asian J. Chem.*, **32**, 2624 (2020); https://doi.org/10.14233/ajchem.2020.22815
49. A.J. Andersson and D. Gledhill, *Annu. Rev. Mar. Sci.*, **5**, 321 (2013); https://doi.org/10.1146/annurev-marine-121211-172241
50. Y.H. Song, J.C. Park, C.S. Kim, D.S. Hwang, H.J. Cha and J.H. Seo, *Biotechnol. Bioprocess Eng.; BBE*, **23**, 341 (2018); https://doi.org/10.1007/s12257-018-0118-7
51. V. Ramasamy, P. Anand and G. Suresh, *Int. J. Mater. Sci.*, **12**, 499 (2017).
52. H.A. Tajmir-Riahi, *J. Inorg. Biochem.*, **31**, 255 (1987); https://doi.org/10.1016/0162-0134(87)80080-6
53. H.A. Tajmir-Riahi, *J. Inorg. Biochem.*, **27**, 123 (1986); https://doi.org/10.1016/0162-0134(86)80013-7
54. S. Alibeigi and M.R. Vaezi, *Chem. Eng. Technol.*, **31**, 1591 (2008); https://doi.org/10.1002/ceat.200800093
55. D. Sivakumar, M. Mohamed Rafi, B. Sathyaseelan, K.M. Prem Nazeer and A.M. Ayisha Begam, *Int. J. Nanodimens.*, **8**, 257 (2017).
56. W. Agudelo, Y. Montoya and J. Bustamante, *Dyna*, **85**, 69 (2018); https://doi.org/10.15446/dyna.v85n206.72136
57. M. Kumari, C.U. Pittman Jr. and D. Mohan, *J. Colloid Interface Sci.*, **442**, 120 (2015); https://doi.org/10.1016/j.jcis.2014.09.012
58. C.S. Doyle, T. Kendelewicz and G.E. Brown Jr., *Appl. Surf. Sci.*, **230**, 260 (2004); https://doi.org/10.1016/j.apsusc.2004.02.035
59. E. Hao, G.C. Schatz and J.T. Hupp, *J. Fluoresc.*, **14**, 331 (2004); https://doi.org/10.1023/B:JOFL.0000031815.71450.74
60. E. Filippo, A. Serra and D. Manno, *Colloids Surf. A Physicochem. Eng. Asp.*, **348**, 205 (2009); https://doi.org/10.1016/j.colsurfa.2009.07.023
61. W. Yang, F. Gao, G. Wei and L. An, *Cryst. Growth Des.*, **10**, 29 (2010); https://doi.org/10.1021/cg901148q
62. H. El Ghandoor, H.M. Zidan, M.M.H. Khalil and M.I.M. Ismail, *Int. J. Electrochem. Sci.*, **7**, 5734 (2012).
63. H. Zhou, B. Yan, J. Lai, H. Liu, A. Ma, W. Chen, X. Jin, W. Zhao and G. Zhang, *J. Ind. Eng. Chem.*, **58**, 334 (2018); https://doi.org/10.1016/j.jiec.2017.09.046
64. H. Liu and C. Di Valentin, *J. Phys. Chem. C*, **121**, 25736 (2017); https://doi.org/10.1021/acs.jpcc.7b09387
65. S.K. Kulkarni, Nanotechnology: Principles and Practices, Capital Publishing Company, New Delhi, edn 1 (2007).
66. S. Rajput, C.U. Pittman Jr. and D. Mohan, *J. Colloid Interface Sci.*, **468**, 334 (2016); https://doi.org/10.1016/j.jcis.2015.12.008
67. J. Zhang, *Sep. Purif. Technol.*, **229**, 115832 (2019); https://doi.org/10.1016/j.seppur.2019.115832
68. Q. Hu, Q. Wang, C. Feng, Z. Zhang, Z. Lei, and K. Shimizu, *J. Mol. Liq.*, **254**, 20 (2018); https://doi.org/10.1016/j.molliq.2018.01.073
69. W. Plazinski, W. Rudzinski and A. Plazinska, *Adv. Colloid Interface Sci.*, **152**, 2 (2009); https://doi.org/10.1016/j.cis.2009.07.009
70. G.Q. Wang, X.G. Yuan and K.T. Yu, *Ind. Eng. Chem. Res.*, **44**, 8715 (2005); https://doi.org/10.1021/ie050017w
71. A.U. Itodo, F.W. Abdulrahman, L.G. Hassan, S.A. Maigandi and H.U. Itodo, *Researcher*, **2**, 74 (2010).
72. C.R. Girish and V.R. Murty, *Int. J. Chem. Eng.*, **2016**, 1 (2016); https://doi.org/10.1155/2016/5809505
73. A. Nimibofa, E. Tobin, S. David, W. Donbebe and D. Dixon, *Hem. Ind. Ind.*, **71**, 429 (2017); https://doi.org/10.2298/HEMIND150608005N
74. X. Chen, *Inf.*, **6**, 14 (2015); https://doi.org/10.3390/info6010014
75. N. Ayawei, A.N. Ebelegi and D. Wankasi, *J. Chem.*, **2017**, 1 (2017); https://doi.org/10.1155/2017/3039817
76. S. Liu, *J. Colloid Interface Sci.*, **450**, 224 (2015); https://doi.org/10.1016/j.jcis.2015.03.013
77. E.L. Morifi, A.E. Ofomaja and K. Pillay, *J. Environ. Chem. Eng.*, **8**, 103822 (2020); https://doi.org/10.1016/j.jece.2020.103822
78. Q. Hu and Z. Zhang, *J. Mol. Liq.*, **277**, 646 (2019); https://doi.org/10.1016/j.molliq.2019.01.005
79. A.N. Ebelegi, N. Ayawei and D. Wankasi, *Open J. Phys. Chem.*, **10**, 166 (2020); https://doi.org/10.4236/ojpc.2020.103010
80. A.L. Myers, *AIChE J.*, **48**, 145 (2002); https://doi.org/10.1002/aic.690480115
81. N.D. Shooto, *Surf. Interfaces*, **20**, 100624 (2020); https://doi.org/10.1016/j.surfin.2020.100624
82. L. Giraldo, A. Erto and J.C. Moreno-Piraján, *Adsorption*, **19**, 465 (2013); https://doi.org/10.1007/s10450-012-9468-1
83. V.E. Pakade, T.D. Ntuli and A.E. Ofomaja, *Appl. Water Sci.*, **7**, 3015 (2017); https://doi.org/10.1007/s13201-016-0412-5
84. P.M. Thabede, N.D. Shooto, T. Xaba and E.B. Naidoo, *J. Environ. Chem. Eng.*, **8**, 104045 (2020); https://doi.org/10.1016/j.jece.2020.104045
85. Y. Bagbi, A. Sarswat, D. Mohan, A. Pandey and P.R. Solanki, *J. Environ. Chem. Eng.*, **4**, 4237 (2016); https://doi.org/10.1016/j.jece.2016.09.026
86. A.R. Mahdavian and M.A.S. Mirrahimi, *Chem. Eng. J.*, **159**, 264 (2010); https://doi.org/10.1016/j.cej.2010.02.041
87. L.P. Lingamdinne, J.R. Koduru and R.R. Karri, Green Synthesis of Iron Oxide Nanoparticles for Lead Removal from Aqueous Solutions, Intech. Open, vol. 805, no. III, pp. 122–127 (2019); https://doi.org/10.4028/www.scientific.net/KEM.805.122